

The study of lepton EDMs in $U(1)_X$ SSM

Lu-Hao Su^{1,2*}, Dan He^{1,2†}, Xing-Xing Dong^{1,2‡}, Tai-Fu Feng^{1,2,3§}, Shu-Min Zhao^{1,2¶}

¹ Department of Physics, Hebei University, Baoding 071002, China

² Key Laboratory of High-precision Computation and Application of Quantum Field Theory of Hebei Province, Baoding 071002, China and

³ Department of Physics, Chongqing University, Chongqing 401331, China

Abstract

The minimal supersymmetric extension of the standard model (MSSM) is extended to the $U(1)_X$ SSM, whose local gauge group is $SU(3)_C \times SU(2)_L \times U(1)_Y \times U(1)_X$. To obtain the $U(1)_X$ SSM, we add the new superfields to the MSSM, namely: three Higgs singlets $\hat{\eta}$, $\hat{\bar{\eta}}$, \hat{S} and right-handed neutrinos $\hat{\nu}_i$. The CP violating effects are considered to study the lepton electric dipole moment(EDM) in $U(1)_X$ SSM. The CP violating phases in $U(1)_X$ SSM are more than those in the standard model(SM). In this model, some new parameters ($\theta_S, \theta_{BB'}, \theta_{BL}$) as CP violating phases are considered, so there are new contributions to lepton EDMs. It is conducive to exploring the source of CP violation and probing new physical beyond SM.

PACS numbers:

Keywords: lepton, electric dipole moment

* suluha00606@163.com

† hedandeya@163.com

‡ dxx_0304@163.com

§ fengtf@hbu.edu.cn

¶ zhaosm@hbu.edu.cn

I. INTRODUCTION

In 1964, Cronin and Fitch discovered the charge conjugate and parity (CP) violating by the decays of the K meson [1]. The study of the lepton electric dipole moments (EDMs) becomes the physical quantities for probing sources of CP violation[2]. Therefore, it is of special significance to research the EDMs of lepton. At present, the upper bound of electron EDM is $|d_e^{exp}| < 1.1 \times 10^{-29}$ e.cm at the 90% confidence level[3–5], the muon EDM is $|d_\mu^{exp}| < 1.8 \times 10^{-19}$ e.cm at the 95% confidence level and the tau EDM is $|d_\tau^{exp}| < 1.1 \times 10^{-17}$ e.cm at the 95% confidence level [6]. The sources and mechanism of CP violation have not been well explained. Scientists are trying to find CP violation terms in new physics beyond SM in order to better explain CP violation mechanism[7–10]. There are several CP violating phases, which can give large contributions to the EDMs of lepton in the minimal supersymmetric extension of standard model (MSSM)[11–14].

Due to the deficiency of MSSM which can not explain neutrino mass and not solve μ problem, $U(1)$ extension of MSSM is carried out. There are two $U(1)$ groups in $U(1)_X$ SSM: $U(1)_Y$ and $U(1)_X$, and the $U(1)_X$ SSM is explored that we use SARAH software packages [15–17]. By adding some new superfields to MSSM, the $U(1)_X$ SSM not only obtains additional Higgs, neutrino and gauge fields, but corresponding superpartners that extend the neutralino and sfermion sectors. The mass m_{h_0} of the lightest CP-even Higgs [18, 19] in $U(1)_X$ SSM is larger than the corresponding mass in MSSM at tree order. Therefore, In $U(1)_X$ SSM, the loop diagram correction of m_{h_0} does not need to be very large.

It is an effective way to explore new physics beyond the standard model(SM) that research the MDMs [20, 21] and EDMs [22–28] of lepton. The one-loop correction and the two-loop correction to EDM of leptons are well researched in MSSM. d_e in the SM is studied independently of the model[29, 30]. The authors consider the right-handed neutrinos, the neutrino see-saw mechanism and the structure of minimal flavor violation. The results show that when the neutrinos are Majorana particles, the value of d_e will reach the upper limit of the experiment.

In the following, we introduce the specific form of $U(1)_X$ SSM and its superfields in section 2. In section 3, we show that the one-loop and two-loop corrections to the lepton EDMs.

The main content of section 4 is the numerical analysis for the dependence of lepton EDMs on the $U(1)_X$ SSM parameters. We have a special summary and discussion in section 5. The appendix is used for the some mass matrices.

II. THE $U(1)_X$ SSM

The $U(1)_X$ SSM has been expanded on the basis of the MSSM. The $U(1)_X$ SSM superfields include three Higgs singlets $\hat{\eta}$, $\hat{\bar{\eta}}$, \hat{S} and right-handed neutrinos $\hat{\nu}_i$. By the see-saw mechanism, the light neutrinos can get tiny masses at the tree level. For details of the mass matrix of particles, please see the Ref.[31].

The superpotential of $U(1)_X$ SSM is

$$W = l_W \hat{S} + \mu \hat{H}_u \hat{H}_d + M_S \hat{S} \hat{S} - Y_d \hat{d} \hat{q} \hat{H}_d - Y_e \hat{e} \hat{l} \hat{H}_d + \lambda_H \hat{S} \hat{H}_u \hat{H}_d + \lambda_C \hat{S} \hat{\eta} \hat{\bar{\eta}} + \frac{\kappa}{3} \hat{S} \hat{S} \hat{S} + Y_u \hat{u} \hat{q} \hat{H}_u + Y_X \hat{\nu} \hat{\eta} \hat{\bar{\nu}} + Y_\nu \hat{\nu} \hat{l} \hat{H}_u . \quad (1)$$

These two Higgs doublets and three Higgs singlets are shown below in concrete form,

$$\begin{aligned} H_u &= \begin{pmatrix} H_u^+ \\ \frac{1}{\sqrt{2}}(v_u + H_u^0 + iP_u^0) \end{pmatrix}, & H_d &= \begin{pmatrix} \frac{1}{\sqrt{2}}(v_d + H_d^0 + iP_d^0) \\ H_d^- \end{pmatrix}, \\ \eta &= \frac{1}{\sqrt{2}}(v_\eta + \phi_\eta^0 + iP_\eta^0), & \bar{\eta} &= \frac{1}{\sqrt{2}}(v_{\bar{\eta}} + \phi_{\bar{\eta}}^0 + iP_{\bar{\eta}}^0), \\ S &= \frac{1}{\sqrt{2}}(v_S + \phi_S^0 + iP_S^0). \end{aligned} \quad (2)$$

v_u , v_d , v_η , $v_{\bar{\eta}}$ and v_S are the VEVs of the Higgs superfields H_u , H_d , η , $\bar{\eta}$ and S respectively.

Here, we set $\tan \beta = v_u/v_d$ and $\tan \beta_\eta = v_{\bar{\eta}}/v_\eta$. The specific form of $\tilde{\nu}_L$ and $\tilde{\nu}_R$ are

$$\tilde{\nu}_L = \frac{1}{\sqrt{2}}\phi_l + \frac{i}{\sqrt{2}}\sigma_l, \quad \tilde{\nu}_R = \frac{1}{\sqrt{2}}\phi_R + \frac{i}{\sqrt{2}}\sigma_R. \quad (3)$$

The specific form of soft SUSY breaking terms are shown below

$$\begin{aligned} \mathcal{L}_{soft} &= \mathcal{L}_{soft}^{MSSM} - B_S S^2 - L_S S - \frac{T_\kappa}{3} S^3 - T_{\lambda_C} S \eta \bar{\eta} + \epsilon_{ij} T_{\lambda_H} S H_d^i H_u^j \\ &\quad - T_X^{IJ} \bar{\eta} \tilde{\nu}_R^{I*} \tilde{\nu}_R^{*J} + \epsilon_{ij} T_\nu^{IJ} H_u^i \tilde{\nu}_R^{I*} \tilde{l}_j^J - m_\eta^2 |\eta|^2 - m_{\bar{\eta}}^2 |\bar{\eta}|^2 \\ &\quad - m_S^2 S^2 - (m_{\tilde{\nu}_R}^2)^{IJ} \tilde{\nu}_R^{I*} \tilde{\nu}_R^J - \frac{1}{2} \left(M_S \lambda_{\tilde{X}}^2 + 2 M_{BB'} \lambda_{\tilde{B}} \lambda_{\tilde{X}} \right) + h.c.. \end{aligned} \quad (4)$$

The particle content and charge assignments for $U(1)_X$ SSM are shown in the Table I. Compared to the SM, the anomalies of $U(1)_X$ SSM are more complex [32]. This model has been proven anomaly free [31] at last. The two Abelian groups $U(1)_Y$ and $U(1)_X$ in $U(1)_X$ SSM can create a new effect, the gauge kinetic mixing. This effect can also be induced by RGEs even with zero value at M_{GUT} .

Superfields	$SU(3)_C$	$SU(2)_L$	$U(1)_Y$	$U(1)_X$
\hat{Q}_i	3	2	1/6	0
\hat{u}_i^c	$\bar{3}$	1	-2/3	-1/2
\hat{d}_i^c	$\bar{3}$	1	1/3	1/2
\hat{L}_i	1	2	-1/2	0
\hat{e}_i^c	1	1	1	1/2
$\hat{\nu}_i$	1	1	0	-1/2
\hat{H}_u	1	2	1/2	1/2
\hat{H}_d	1	2	-1/2	-1/2
$\hat{\eta}$	1	1	0	-1
$\hat{\bar{\eta}}$	1	1	0	1
\hat{S}	1	1	0	0

TABLE I: The superfields in $U(1)_X$ SSM.

The general form of the covariant derivative of this model is [33–35]

$$D_\mu = \partial_\mu - i \begin{pmatrix} Y, & X \end{pmatrix} \begin{pmatrix} g_Y, & g'_{YX} \\ g'_{XY}, & g'_X \end{pmatrix} \begin{pmatrix} A_\mu'^Y \\ A_\mu'^X \end{pmatrix}. \quad (5)$$

The $A_\mu'^Y$ and $A_\mu'^X$ represent the gauge fields of $U(1)_Y$ and $U(1)_X$. Since these two Abelian gauge groups are unbroken, we make a basis exchange. Using the orthogonal matrix R [33, 35], the resulting formula is shown below

$$\begin{pmatrix} g_Y, & g'_{YX} \\ g'_{XY}, & g'_X \end{pmatrix} R^T = \begin{pmatrix} g_1, & g_{YX} \\ 0, & g_X \end{pmatrix}. \quad (6)$$

We deduce $\sin^2 \theta'_W =$

$$\frac{1}{2} - \frac{((g_{YX} + g_X)^2 - g_1^2 - g_2^2)v^2 + 4g_X^2\xi^2}{2\sqrt{((g_{YX} + g_X)^2 + g_1^2 + g_2^2)^2v^4 + 8g_X^2((g_{YX} + g_X)^2 - g_1^2 - g_2^2)v^2\xi^2 + 16g_X^4\xi^4}}. \quad (7)$$

with $\xi = \sqrt{v_\eta^2 + v_{\bar{\eta}}^2}$. The new mixing angle θ'_W can be found in the couplings of Z and Z' .

Next, we describe some of the couplings needed.

The couplings of $\tilde{\nu}_k^R - \bar{e}_i - \chi_j^-$ and $\tilde{\nu}_k^I - \bar{e}_i - \chi_j^-$ are

$$\mathcal{L}_{\tilde{\nu}^R \bar{e} \chi^-} = \bar{e}_i \left\{ \frac{i}{\sqrt{2}} U_{j2}^* Z_{ki}^{R*} Y_e^i P_L - \frac{i}{\sqrt{2}} g_2 V_{j1} Z_{ki}^{R*} P_R \right\} \chi_j^- \tilde{\nu}_k^R, \quad (8)$$

$$\mathcal{L}_{\tilde{\nu}^I \bar{e} \chi^-} = \bar{e}_i \left\{ \frac{-1}{\sqrt{2}} U_{j2}^* Z_{ki}^{I*} Y_e^i P_L + \frac{1}{\sqrt{2}} g_2 V_{j1} Z_{ki}^{I*} P_R \right\} \chi_j^- \tilde{\nu}_k^I. \quad (9)$$

With $P_L = \frac{1-\gamma_5}{2}$ and $P_R = \frac{1+\gamma_5}{2}$. Z^R and Z^I are rotation matrices, which can diagonalize the mass squared matrices of CP-even sneutrino and CP-odd sneutrino. The mass matrix for chargino is diagonalized by rotation matrices U and V .

We also deduce the vertex couplings of neutrino-slepton-chargino and neutralino-lepton-slepton,

$$\begin{aligned} \mathcal{L}_{\bar{\nu} \chi^- \tilde{L}} &= \bar{\nu}_i \left((-g_2 U_{j1}^* \sum_{a=1}^3 U_{ia}^{V*} Z_{ka}^E + U_{j2}^* \sum_{a=1}^3 U_{ia}^{V*} Y_l^a Z_{k(3+a)}^E) P_L \right. \\ &\quad \left. + \sum_{a,b=1}^3 Y_\nu^{ab} U_{i(3+a)}^V Z_{kb}^E V_{j2} P_R \right) \chi_j^- \tilde{L}_k, \end{aligned} \quad (10)$$

$$\begin{aligned} \mathcal{L}_{\bar{\chi}^0 l \tilde{L}} &= \bar{\chi}_i^0 \left\{ \left(\frac{1}{\sqrt{2}} (g_1 N_{i1}^* + g_2 N_{i2}^* + g_{YX} N_{i5}^*) Z_{kj}^E - N_{i3}^* Y_l^j Z_{k(3+j)}^E \right) P_L \right. \\ &\quad \left. - \left[\frac{1}{\sqrt{2}} (2g_1 N_{i1} + (2g_{YX} + g_X) N_{i5}) Z_{k(3+a)}^E + Y_l^j Z_{kj}^E N_{i3} \right] P_R \right\} l_j \tilde{L}_k. \end{aligned} \quad (11)$$

With Z^E and N are rotation matrices, which can diagonalize the mass squared matrix of slepton and the mass matrix of neutralino. The mass matrix for neutrino is diagonalized by U^V .

Other couplings needed can be found in our previous works [31, 36].

III. FORMULATION

The Feynman amplitude can be expressed by these dimension 6 operators [37] with the effective Lagrangian method. The dimension 8 operators be suppressed by the factor $\frac{m_\mu^2}{M_{SUSY}^2}$

$\sim (10^{-7}, 10^{-8})$ and can then be ignored.

These dimension 6 operators are shown below

$$\begin{aligned}\mathcal{O}_1^\mp &= \frac{1}{(4\pi)^2} \bar{l}(i\mathcal{D})^3 \omega_\mp l , \\ \mathcal{O}_2^\mp &= \frac{eQ_f}{(4\pi)^2} \overline{(i\mathcal{D}_\mu l)} \gamma^\mu F \cdot \sigma \omega_\mp l , \\ \mathcal{O}_3^\mp &= \frac{eQ_f}{(4\pi)^2} \bar{l} F \cdot \sigma \gamma^\mu \omega_\mp (i\mathcal{D}_\mu l) , \\ \mathcal{O}_4^\mp &= \frac{eQ_f}{(4\pi)^2} \bar{l} (\partial^\mu F_{\mu\nu}) \gamma^\nu \omega_\mp l , \\ \mathcal{O}_5^\mp &= \frac{m_l}{(4\pi)^2} \bar{l}(i\mathcal{D})^2 \omega_\mp l , \\ \mathcal{O}_6^\mp &= \frac{eQ_f m_l}{(4\pi)^2} \bar{l} F \cdot \sigma \omega_\mp l .\end{aligned}\tag{12}$$

Here, $\mathcal{D}_\mu = \partial_\mu + ieA_\mu$ and $\omega_\mp = \frac{1 \mp \gamma_5}{2}$. $F_{\mu\nu}$ denotes the electromagnetic field strength, and m_l represents the lepton mass.

The effective Lagrangian of lepton EDM is

$$\mathcal{L}_{EDM} = \frac{-i}{2} d_l \bar{l} \sigma^{\mu\nu} \gamma_5 l F_{\mu\nu} .\tag{13}$$

For Fermions EDM cannot be obtained at tree level in the fundamental interaction because it is a CP violation amplitude. Then, the one-loop diagrams should have non-zero contribution to Fermion EDM in the CP violating electroweak theory. With the relationship between the Wilson coefficients $C_{2,3,6}^\mp$ of the operators $\mathcal{O}_{2,3,6}^\mp$ [26–28, 37], the lepton EDM obtained is shown below

$$d_l = \frac{-2eQ_f m_l}{(4\pi)^2} \Im(C_2^+ + C_2^{-*} + C_6^+) .\tag{14}$$

A. The one-loop corrections

The one-loop new physics contributions to lepton EDMs come from the diagrams in FIG.

1. The one-loop contributions to lepton EDMs are obtained by calculating with the on-shell condition of external lepton. Then we simplify the analytical results.

The analytical results of the one-loop diagrams are shown below

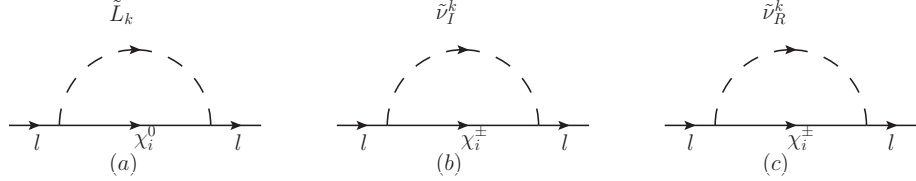


FIG. 1: The one-loop self energy diagrams in the $U(1)_X$ SSM.

1. The corrections to lepton EDMs from neutralinos and scalar leptons are

$$d_l^{\tilde{L}\chi^0} = \left(\frac{-e}{2\Lambda}\right) \Im \left[- \sum_{i=1}^8 \sum_{j=1}^6 \left\{ (A_L^* A_R) \sqrt{x_{\chi_i^0}} x_{\tilde{L}_j} \frac{\partial^2 \mathcal{B}(x_{\chi_i^0}, x_{\tilde{L}_j})}{\partial x_{\tilde{L}_j}^2} \right\} \right]. \quad (15)$$

With $x_i = \frac{m_i^2}{\Lambda^2}$, m_i represents the particle mass and Λ denotes the new physics energy scale.

The couplings A_R, A_L can be expressed as

$$\begin{aligned} A_R &= \frac{1}{\sqrt{2}} g_1 N_{i1}^* Z_{j2}^E + \frac{1}{\sqrt{2}} g_2 N_{i2}^* Z_{j2}^E + \frac{1}{\sqrt{2}} g_{YX} N_{i5}^* Z_{j2}^E - N_{i3}^* Y_\mu Z_{j5}^E, \\ A_L &= -\frac{1}{\sqrt{2}} Z_{j5}^E (2g_1 N_{i1} + (2g_{YX} + g_X) N_{i5}) - Y_\mu^* Z_{j2}^E N_{i3}. \end{aligned} \quad (16)$$

The mass matrices of scalar leptons and neutrinos can be diagonalized using the matrices Z^E and N .

The specific forms of functions $\mathcal{B}(x, y)$ (using in the Eq.(11)) and $\mathcal{B}_1(x, y)$ (using in the Eqs.(14) and (16)) are shown below

$$\mathcal{B}(x, y) = \frac{1}{16\pi^2} \left(\frac{x \ln x}{y - x} + \frac{y \ln y}{x - y} \right), \quad \mathcal{B}_1(x, y) = \left(\frac{\partial}{\partial y} + \frac{y}{2} \frac{\partial^2}{\partial y^2} \right) \mathcal{B}(x, y). \quad (17)$$

2. The corrections from chargino and CP-odd scalar neutrino are

$$d_{lI}^{\tilde{\nu}\chi^\pm} = \left(\frac{-e}{2\Lambda}\right) \Im \left[\sum_{i=1}^2 \sum_{j=1}^6 \left\{ -2(B_L^* B_R) \sqrt{x_{\chi_i^-}} \mathcal{B}_1(x_{\tilde{\nu}_j^I}, x_{\chi_i^-}) \right\} \right]. \quad (18)$$

The couplings B_L and B_R can be expressed as

$$B_L = -\frac{1}{\sqrt{2}} U_{i2}^* Z_{j2}^{I*} Y_\mu, \quad B_R = \frac{1}{\sqrt{2}} g_2 Z_{j2}^{I*} V_{i1}. \quad (19)$$

3. The corrections from chargino and CP-even scalar neutrino are

$$d_{lR}^{\tilde{\nu}\chi^\pm} = \left(\frac{-e}{2\Lambda}\right) \Im \left[\sum_{i=1}^2 \sum_{j=1}^6 \left\{ -2(C_L^* C_R) \sqrt{x_{\chi_i^-}} \mathcal{B}_1(x_{\tilde{\nu}_j^R}, x_{\chi_i^-}) \right\} \right]. \quad (20)$$

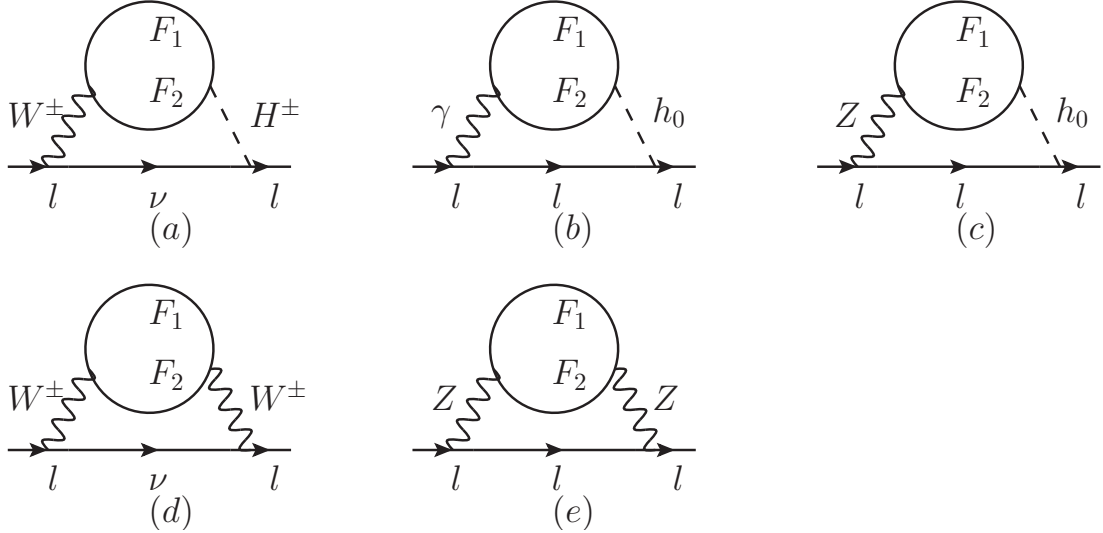


FIG. 2: The two-loop Barr-Zee and rainbow type diagrams in the $U(1)_X$ SSM.

The couplings C_L and C_R can be expressed as

$$C_L = \frac{1}{\sqrt{2}} U_{i2}^* Z_{j2}^{R*} Y_\mu , \quad C_R = -\frac{1}{\sqrt{2}} g_2 Z_{j2}^{R*} V_{i1} . \quad (21)$$

And, the U , V , Z^R and Z^I matrices diagonalize the corresponding particle mass matrices, which are detailed in the appendix.

So the contributions of the one-loop diagrams to lepton EDMs are

$$d_l^{one-loop} = d_l^{\tilde{L}\chi^0} + d_{lI}^{\tilde{\nu}\chi^\pm} + d_{lR}^{\tilde{\nu}\chi^\pm} . \quad (22)$$

B. The two-loop corrections

In this paper, the two-loop diagrams that we research include the Barr-Zee two-loop diagrams (FIG. 2 (a), (b), (c)) and rainbow two-loop diagrams (FIG. 2 (d), (e)), as shown below.

The analytical results of the contributions from the two-loop diagrams to lepton EDMs are shown below.

The contribution from FIG. 2 (a). Under the assumption $m_F = m_{F_1} = m_{F_2} \gg m_W$, the

result [38] of simplification is

$$d_l^{WH} = \frac{-G_F m_W^2 s_W}{256\pi^4} \sum_{F_1=\chi^\pm} \sum_{F_2=\chi^0} \frac{H_{lH\nu}^L}{m_F} \left\{ \Im \left[\left[\frac{21}{4} - \frac{5}{18} Q_{F_1} + \left(3 + \frac{Q_{F_1}}{3} \right) (\ln m_{F_1}^2 - \varrho_{1,1}(m_W^2, m_{H^\pm}^2)) \right] (H_{HF_1F_2}^L H_{WF_1F_2}^L + H_{HF_1F_2}^R H_{WF_1F_2}^R) + \left[\frac{19 - 20Q_{F_1}}{9} + \frac{2 - 4Q_{F_1}}{3} (\ln m_{F_1}^2 - \varrho_{1,1}(m_W^2, m_{H^\pm}^2)) \right] (H_{HF_1F_2}^L H_{WF_1F_2}^R + H_{HF_1F_2}^R H_{WF_1F_2}^L) + \left[-\frac{16}{9} - \frac{2+6Q_{F_1}}{3} (\ln m_{F_1}^2 - \varrho_{1,1}(m_W^2, m_{H^\pm}^2)) \right] (H_{HF_1F_2}^L H_{WF_1F_2}^L - H_{HF_1F_2}^R H_{WF_1F_2}^R) + \left[-\frac{2Q_{F_1}}{9} - \frac{6-2Q_{F_1}}{3} (\ln m_{F_1}^2 - \varrho_{1,1}(m_W^2, m_{H^\pm}^2)) \right] (H_{HF_1F_2}^L H_{WF_1F_2}^R - H_{HF_1F_2}^R H_{WF_1F_2}^L) \right] \right\}. \quad (23)$$

Here, $\varrho_{1,1}(x, y) = \frac{x \ln x - y \ln y}{x-y}$. $H_{HF_1F_2}^{L,R}$ and $H_{WF_1F_2}^{L,R}$ denote the corresponding couplings coefficients. Please see the Ref.[36] for their concrete forms.

Under the assumption $m_F = m_{F_1} = m_{F_2} \gg m_{h_0}$, the reduced form of the contribution to lepton EDM from FIG. 2(b) is

$$d_l^{h_0} = \frac{-e G_F Q_f Q_{F_1} m_W^2 s_W^2}{32\pi^4} \sum_{F_1=F_2=\chi^\pm} \left\{ \Im \left[\frac{1}{m_{F_1}} (H_{h_0 F_1 F_2}^L) [1 + \ln \frac{m_{F_1}^2}{m_{h_0}^2}] \right] \right\}. \quad (24)$$

And, the simplified form from FIG. 2(c) is given below

$$d_l^{Z h_0} = \frac{-\sqrt{2} e}{1024\pi^4} \sum_{F_1=F_2=\chi^\pm, \chi^0} \left\{ \frac{H_{h_0 l\bar{l}}}{m_{F_1}} \left[\varrho_{1,1}(m_Z^2, m_{h_0}^2) - \ln m_{F_1}^2 - 1 \right] \times \Im [(H_{Zll}^L - H_{Zll}^R) (H_{h_0 F_1 F_2}^L H_{ZF_1 F_2}^L + H_{h_0 F_1 F_2}^R H_{ZF_1 F_2}^R)] \right\}. \quad (25)$$

With Q_f represents the electric charge of the external lepton m_μ . Q_{F_1} and Q_{F_2} denote the electric charges of the internal charginos.

With the assumption $m_F = m_{F_1} = m_{F_2} \gg m_W \sim m_Z$, the reduced form of the contribution to lepton EDM from FIG. 2(d) is

$$d_l^{WW} = \frac{-e G_F m_l}{384\sqrt{2}\pi^4} \sum_{F_1=\chi^\pm} \sum_{F_2=\chi^0} \left\{ \Im [11(H_{WF_1F_2}^{R*} H_{WF_1F_2}^L)] \right\}. \quad (26)$$

We simplify the tedious two-loop results to the order $\frac{m_\mu^2}{M_Z^2} \sim 10^{-6}$ or $\frac{m_\mu^2}{m_{SUSY}^2}$ under the assumption $m_F = m_{F_1} = m_{F_2} \gg m_W \sim m_Z$, and get the simplified form of FIG. 2(e) as follows

$$d_l^{ZZ} = \frac{eQ_{F_1}m_l}{2048\Lambda^2\pi^4} \sum_{F_1=F_2=\chi^\pm} \left\{ \Im \left[(H_{Z F_1 F_2}^L H_{Z F_1 F_2}^R) \left(|H_{Zll}^L|^2 + |H_{Zll}^R|^2 \right) \left[\frac{-6 \log x_Z + 6 \log x_F + 4}{9x_F} \right] \right. \right. \\ \left. \left. + \left(|H_{Z F_1 F_2}^L|^2 + |H_{Z F_1 F_2}^R|^2 \right) H_{Zll}^L H_{Zll}^R [16 \frac{(\log x_F - \log x_Z)(\log x_F + 2) + 2}{x_Z}] \right] \right\}. \quad (27)$$

The contributions to lepton EDMs from the researched two-loop diagrams are

$$d_l^{two-loop} = d_l^{WH} + d_l^{\gamma h_0} + d_l^{Zh_0} + d_l^{WW} + d_l^{ZZ}. \quad (28)$$

At two-loop level, the contributions to lepton EDMs can be summarized as

$$d_l^{total} = d_l^{one-loop} + d_l^{two-loop}. \quad (29)$$

IV. THE NUMERICAL RESULTS

For the numerical discussion, we consider the following experimental limitations. The lightest CP-even higgs mass is considered as an input parameter, which is $m_{h^0} \approx 125.1$ GeV [39, 40]. And h^0 decays are $h^0 \rightarrow \gamma + \gamma$, $h^0 \rightarrow Z + Z$ and $h^0 \rightarrow \gamma + \gamma$ [41]. Experimental constraints on the masses of the new particles are also considered. The LHC experiments have more stringent mass constraints on Z' boson. To satisfy the experimental constraint, we take the parameter $M_{Z'}$ greater than 5.1 TeV [42], which is heavier than the previous mass limit. The ratio of $M_{Z'}$ to its gauge coupling g_X , $(\frac{M_{Z'}}{g_X})$ should be not less than 6 TeV at 99% C.L. [43, 44]. Considering the constraints from the LHC, we set the $\tan \beta_\eta < 1.5$ [45]. Since $M_{Z'}$ has a large mass, the contribution of Z' at the amplitude level is very small, so the contribution of Z' is ignored. Considering the experimental limitation of lepton EDMs, we adjust the parameters. In this section, we research and discuss lepton (e, μ, τ)EDMs respectively.

The parameters used in $U(1)_X$ SSM are given below:

$$\begin{aligned}
g_X &= 0.33, \quad g_{YX} = 0.2, \quad \lambda_C = -0.1, \quad \kappa = 0.1, \quad T_{\lambda_H} = 1.0 \text{ TeV}, \quad T_\kappa = 1.0 \text{ TeV}, \\
\tan \beta_\eta &= 1.05, \quad v_\eta = 15 \times \cos \beta_\eta \text{ TeV}, \quad v_{\bar{\eta}} = 15 \times \sin \beta_\eta \text{ TeV}, \quad B_\mu = 8 \text{ TeV}^2, \\
m_S^2 &= 8 \text{ TeV}^2, \quad T_{\lambda_C} = 150 \text{ GeV}, \quad T_{E11} = T_{E22} = T_{E33} = 0.1 \text{ TeV}, \\
M_{\nu11} &= M_{\nu22} = M_{\nu33} = 6 \text{ TeV}^2, \quad Y_{X11} = Y_{X22} = Y_{X33} = 0.04, \\
B_S &= 8 \text{ TeV}^2, \quad \lambda_H = 0.1, \quad l_W = 8 \text{ TeV}^2, \quad T_{X11} = T_{X22} = T_{X33} = 10 \text{ GeV}. \tag{30}
\end{aligned}$$

θ_1 , θ_2 and θ_μ are the CP violating phases of the parameters m_1 , m_2 and μ . We take into account three new CP violating parameters with the phases θ_{BL} , $\theta_{BB'}$ and θ_S .

$$\begin{aligned}
m_1 &= M_1 * e^{i*\theta_1}, \quad m_2 = M_2 * e^{i*\theta_2}, \quad \mu = mu * e^{i*\theta_\mu}, \\
m_{BL} &= M_{BL} * e^{i*\theta_{BL}}, \quad m_{BB'} = M_{BB'} * e^{i*\theta_{BB'}}, \quad m_S = M_S * e^{i*\theta_S}. \tag{31}
\end{aligned}$$

In order to facilitate the following discussion, we have made some simplifications:

$$\begin{aligned}
M_L &= M_{L11} = M_{L22} = M_{L33}, \quad M_E = M_{E11} = M_{E22} = M_{E33}, \\
T_E &= T_{E11} = T_{E22} = T_{E33}. \tag{32}
\end{aligned}$$

A. the e EDM

At the beginning, we discussed the EDM of electron, because its experimental upper limit is very strict. The CP violating phases θ_1 , θ_2 , θ_μ , θ_{BL} , $\theta_{BB'}$ and θ_S , also including other parameters have a certain impact on the electron EDM. Now, supposing $\theta_1 = \theta_2 = \theta_\mu = \theta_{BB'} = \theta_S = 0$, and setting $\tan \beta = 5$, $M_2 = 500$ GeV, $mu = 500$ GeV, $M_{BL} = 1800$ GeV, $M_{BB'} = 700$ GeV, $M_S = 2400$ GeV, $M_L = 1.1$ TeV, $M_E = 1.0$ TeV. We study the influence of θ_{BL} on electron EDM. M_{BL} is related to neutralino mass matrix. In FIG. 3, we plot the solid line and dashed line versus M_L ($0.9 \sim 1.1$ TeV 2) corresponding to $M_1 = 700, 800$ GeV. We can see that these two lines are subtractive functions, and θ_{BL} has influence on $|d_e|$. The relationship between d_e and M_L is not a simple linear relation, its change curve is like M_L^{-2} . The shaded part of the figure indicates that all these parameters are within reasonable parameters and conform to experimental limits.

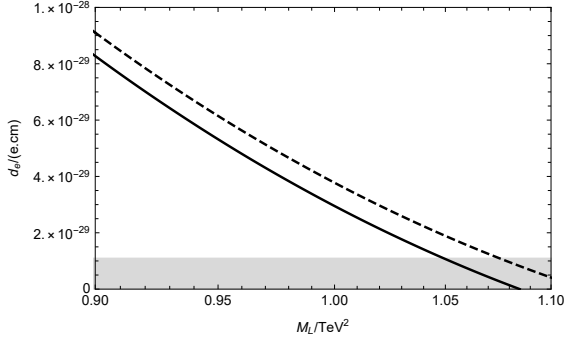


FIG. 3: With $\theta_1 = \theta_2 = \theta_\mu = \theta_{BB'} = \theta_S = 0$, and $\theta_{BL} = \frac{\pi}{4}$, the contributions to electron EDM varying with M_L are plotted by the solid line, dashed line respectively corresponding to $M_1 = (700, 800)$ GeV.

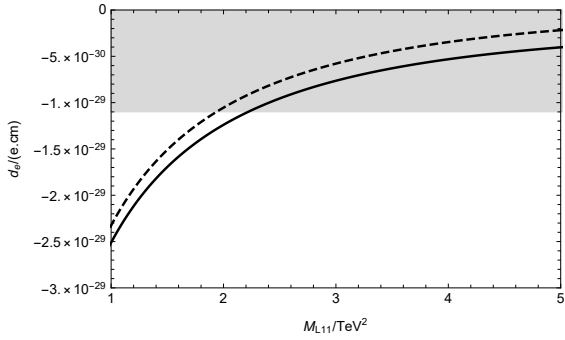


FIG. 4: With $\theta_1 = \theta_2 = \theta_\mu = \theta_{BB'} = \theta_{BL} = 0$, and $\theta_S = \frac{\pi}{4}$, the contributions to electron EDM varying with M_{L11} are plotted by the solid line, dashed line respectively corresponding to $M_{L33} = (1, 0.9)$ TeV 2 .

Setting $\theta_1 = \theta_2 = \theta_\mu = \theta_{BB'} = \theta_{BL} = 0$, $\tan\beta = 5$, $M_1 = 700$ GeV, $M_2 = 2000$ GeV, $mu = 500$ GeV, $M_{BL} = 1600$ GeV, $M_{BB'} = 800$ GeV, $M_S = -800$ GeV, $M_{L22} = 1.0$ TeV 2 , $M_E = 1.0$ TeV 2 , we consider the impact of θ_S on the electron EDM. M_S is related to the mass matrices of neutralino and scalar lepton. In FIG. 4, M_{L11} varies from 0.5 to 5.0 TeV 2 , and when $M_{L11} > 2.0$ TeV 2 , the numerical results of $|d_e|$ conform to the experimental limits.

$\theta_{BB'}$ is the new CP violating phase of the lepton neutrino mass matrix. So, it make new physical contribution to the lepton EDM. With $\theta_1 = \theta_2 = \theta_\mu = \theta_S = \theta_{BL} = 0$, the contributions to muon EDM varying with T_E are plotted by the solid line and dashed line respectively corresponding to $M_{E11} = 0.5$ and 1.0 TeV 2 . In this part, we set $\tan\beta = 5$,

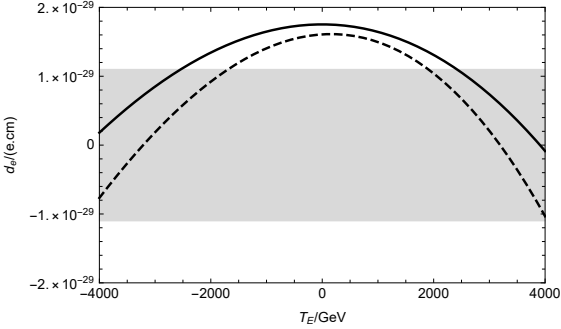


FIG. 5: With $\theta_1 = \theta_2 = \theta_\mu = \theta_S = \theta_{BL} = 0$, and $\theta_{BB'} = \frac{\pi}{3}$, the contributions to electron EDM varying with T_E are plotted by the solid line, dashed line respectively corresponding to $M_{E11} = (0.5, 1.0)$ TeV 2 .

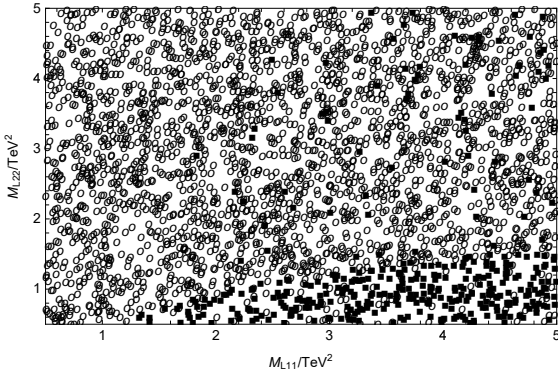


FIG. 6: With $\theta_1 = \theta_2 = \theta_\mu = \theta_{BB'} = \theta_{BL} = 0$, and $\theta_S = \frac{\pi}{4}$, $|d_e|$ is in the plane of M_{L11} versus M_{L22} , “■” represents $|d_e| < 1.1 \times 10^{-29}$ e.cm, “○” represents $|d_e| \geq 1.1 \times 10^{-29}$ e.cm.

$M_1 = 700$ GeV, $M_2 = 2000$ GeV, $mu = 500$ GeV, $M_{BL} = 1800$ GeV, $M_{BB'} = 700$ GeV, $M_S = 2400$ GeV, $M_L = 1.0$ TeV 2 , $M_E = 0.5$ TeV 2 . In FIG. 5, the two lines are shaped like parabolas. And most of the numerical results are within experimental limits.

We select these parameters $M_{L11}(0.5 \sim 5.0$ TeV $^2)$, $M_{L22}(0.5 \sim 5.0$ TeV $^2)$, $M_{L33}(0.5 \sim 5.0$ TeV $^2)$, $T_E(-3000 \sim 3000$ GeV), $M_E(0.5 \sim 5.0$ TeV $^2)$, and randomly scatter points. With $\theta_1 = \theta_2 = \theta_\mu = \theta_{BB'} = \theta_{BL} = 0$, and $\theta_S = \frac{\pi}{4}$. We plot $|d_e|$ in the plane of M_{L11} versus M_{L22} in Fig. 6. “■” represents $|d_e| < 1.1 \times 10^{-29}$ e.cm, “○” represents $|d_e| \geq 1.1 \times 10^{-29}$ e.cm. In Fig. 6, We can see that there is a clear stratification. When $M_{L11} > 1.0$ TeV 2 , M_{L22} is in the vicinity of 1.4 TeV 2 , $|d_e|$ is within the experimental limit. This can show

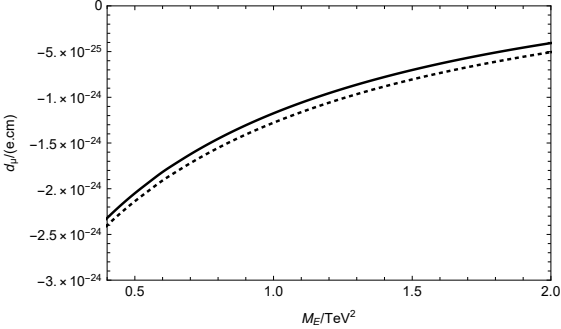


FIG. 7: With $\theta_1 = \theta_2 = \theta_\mu = \theta_{BB'} = \theta_{BL} = 0$, and $\theta_S = \frac{\pi}{3}$, the contributions to muon EDM varying with M_E are plotted by the solid line, dashed line respectively corresponding to $M_{BL} = (1200, 1500)$ GeV.

that M_{L11} is a sensitive parameters and M_{L22} is a less sensitive parameter.

B. the μ EDM

In this section, the muon EDM is numerically studied. In FIG. 7, setting $\theta_1 = \theta_\mu = \theta_{BB'} = \theta_2 = \theta_{BL} = 0$, and setting $\tan\beta = 6$, $M_1 = 1450$ GeV, $M_2 = 2000$ GeV, $mu = 500$ GeV, $M_{BB'} = 800$ GeV, $M_S = -800$ GeV, $M_L = 1.0$ TeV^2 , $M_E = 0.5$ TeV^2 . We study the influence of θ_S on the muon EDM. These solid line, dashed line correspond to M_{BL} (1200, 1500 GeV). We can see that the numerical result of the muon EDM increases as M_E increases. The θ_S has great influence on the numerical results, because of that M_S is related to the mass matrices of neutralino and charge Higgs.

$\theta_{BB'}$ is the new CP violating phase of the neutralino mass matrix. So, it makes new physical contribution to the lepton EDMs. With $\theta_1 = \theta_2 = \theta_\mu = \theta_S = \theta_{BL} = 0$, the contributions to muon EDM varying with M_{E22} are plotted by the solid line and dashed line respectively corresponding to $\tan\beta = (5, 6)$. In this part, we set $M_1 = 1450$ GeV, $M_2 = 800$ GeV, $mu = 500$ GeV, $M_{BL} = 1600$ GeV, $M_{BB'} = 800$ GeV, $M_S = -800$ GeV, $M_L = 1.0$ TeV^2 , $M_E = 0.5$ TeV^2 . In FIG. 8, as M_{E22} increasing, the numerical result decreases slowly, and the shapes of the two lines are similar.

We choose these parameters $M_{L11}(0.5 \sim 5.0 \text{ TeV}^2)$, $M_{L22}(0.5 \sim 5.0 \text{ TeV}^2)$, $M_{L33}(0.5 \sim$

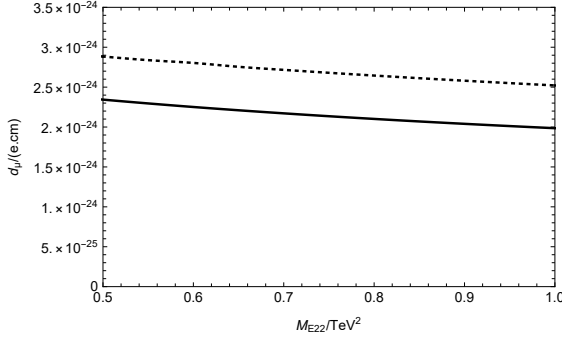


FIG. 8: With $\theta_1 = \theta_2 = \theta_\mu = \theta_S = \theta_{BL} = 0$, and $\theta_{BB'} = \frac{\pi}{6}$, the contributions to muon EDM varying with M_{E22} are plotted by the solid line, dashed line respectively corresponding to $\tan\beta = (5, 6)$.

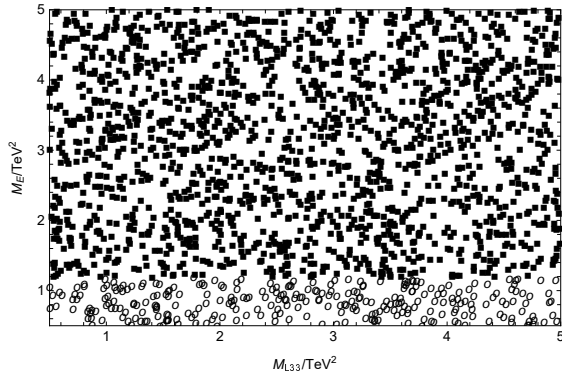


FIG. 9: With $\theta_1 = \theta_2 = \theta_\mu = \theta_{BB'} = \theta_{BL} = 0$, and $\theta_S = \frac{\pi}{4}$, $|d_\mu|$ is in the plane of M_{L33} versus M_E , “■” represents $|d_\mu| < 1 \times 10^{-24}$ e.cm, “○” represents $|d_\mu| \geq 1 \times 10^{-24}$ e.cm.

5.0 TeV^2), $T_E(-3000 \sim 3000 \text{ GeV})$, $M_E(0.5 \sim 5.0 \text{ TeV}^2)$, and randomly scatter points. With $\theta_1 = \theta_2 = \theta_\mu = \theta_{BB'} = \theta_{BL} = 0$, and $\theta_S = \frac{\pi}{4}$, we study $|d_\mu|$ in the plane of M_{L33} versus M_E . In FIG. 9, “■” represents $|d_\mu| < 1 \times 10^{-24}$ e.cm, “○” represents $|d_\mu| \geq 1 \times 10^{-24}$ e.cm. Delamination occurs when $M_E = 1.1 \text{ TeV}^2$, and the stratification is obvious. This can show that M_E is a sensitive parameter and M_{L33} is an insensitive parameter. These parameters are in a reasonable parameter space.

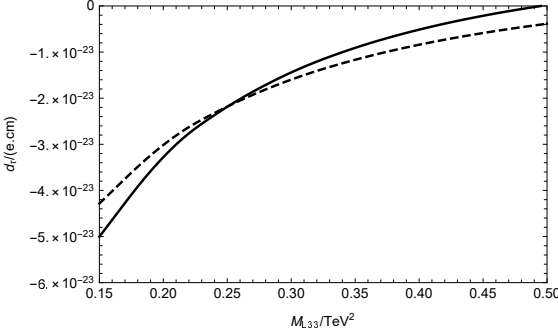


FIG. 10: With $\theta_1 = \theta_2 = \theta_\mu = \theta_{BB'} = \theta_{BL} = 0$, and $\theta_S = \frac{\pi}{5}$, the contributions to tau EDM varying with M_{L33} are plotted by the solid line, dashed line respectively corresponding to $M_2 = (400, 500)$ GeV.

C. the τ EDM

At present, the experimental upper bound of tau EDM is $|d_\tau^{exp}| < 1.1 \times 10^{-17}$ e.cm, and it is largest one among bounds of the lepton EDMs. So, we study the tau EDM in this subsection. Setting $\tan\beta = 6$, $M_1 = 750$ GeV, $mu = 650$ GeV, $M_{BL} = 1800$ GeV, $M_{BB'} = 700$ GeV, $M_S = 1400$ GeV, $M_L = 1.0$ TeV 2 , $M_E = 1.0$ TeV 2 , and setting $\theta_1 = \theta_2 = \theta_\mu = \theta_{BB'} = \theta_{BL} = 0$, and $\theta_S = \frac{\pi}{5}$, we study the influence of M_{L33} on $|d_\tau|$. In FIG. 10, the solid line and dashed line respectively correspond to $M_2 = (400, 500)$ GeV and their numerical results are all in the negative part. The two lines are increasing functions of M_{L33} , and θ_S has more obvious influence on numerical result of $|d_\tau|$. The maximum value of two lines can reach 5.0×10^{-23} e.cm, and this value is 6 orders of magnitude smaller than the upper limit of the experiment.

θ_{BL} is the new CP violating phase of M_{BL} in the neutralino mass matrix. Setting $\tan\beta = 6$, $M_1 = 750$ GeV, $M_2 = 400$ GeV, $M_{BL} = 1800$ GeV, $M_{BB'} = 700$ GeV, $M_S = 1400$ GeV, $M_E = 1.0$ TeV 2 , $\theta_1 = \theta_2 = \theta_\mu = \theta_{BB'} = \theta_S = 0$, and $\theta_{BL} = \frac{\pi}{6}$, the contributions to tau EDM varying with M_L are plotted by the solid line and dashed line respectively corresponding to $mu = (650, 750)$ GeV. In FIG. 11, we can see that $|d_\tau|$ decreases with the increase of M_L . The maximum value of these two lines can reach $|d_\tau| = 4.5 \times 10^{-23}$ e.cm.

We select these parameters $M_{L11}(0.5 \sim 5.0 \text{ TeV}^2)$, $M_{L22}(0.5 \sim 5.0 \text{ TeV}^2)$, $M_{L33}(0.5 \sim$

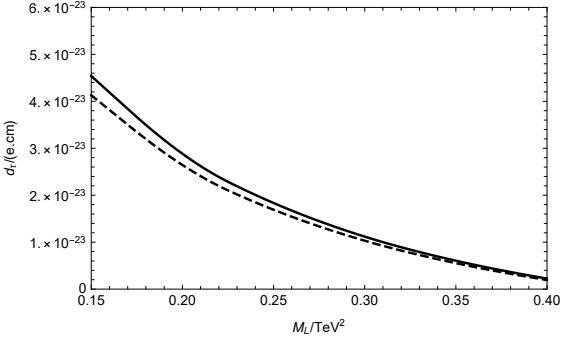


FIG. 11: With $\theta_1 = \theta_2 = \theta_\mu = \theta_S = \theta_{BB'} = 0$, and $\theta_{BL} = \frac{\pi}{6}$, the contributions to tau EDM varying with M_L are plotted by the solid line, dashed line respectively corresponding to $mu = (650, 750)$ GeV.

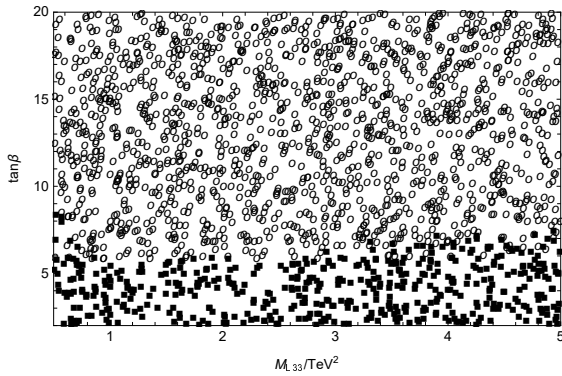


FIG. 12: With $\theta_1 = \theta_2 = \theta_\mu = \theta_{BB'} = \theta_S = 0$, and $\theta_{BL} = \frac{\pi}{6}$, $|d_\tau|$ is in the plane of M_{L33} versus $\tan\beta$, “■” represents $|d_\tau| < 1 \times 10^{-23}$ e.cm, “○” represents $|d_\tau| \geq 1 \times 10^{-23}$ e.cm.

5.0 TeV^2), $T_E(-3000 \sim 3000 \text{ GeV})$, $\tan\beta(2 \sim 20)$, and randomly scatter points. In Fig. 12, we study $|d_\tau|$ in the plane of M_{L33} and $\tan\beta$ to see their influence. The varying regions of M_{L33} and $\tan\beta$ are in the range ($0.5 \sim 5 \text{ TeV}^2$) and ($2 \sim 20$) respectively. “■” represents $|d_\tau| < 1 \times 10^{-23}$ e.cm, “○” represents $|d_\tau| \geq 1 \times 10^{-23}$ e.cm. When $\tan\beta = 6$, stratification occurs, and the stratification is more obvious. This indicates that $\tan\beta$ is a sensitive parameter.

V. DISCUSSION AND CONCLUSION

In the $U(1)_X$ SSM, we calculate and analyze the one-loop and two-loop contributions to the lepton (e, μ, τ) EDMs. The effects of the CP violating phases $\theta_1, \theta_2, \theta_\mu, \theta_{BB'}, \theta_S, \theta_{BL}$ to the lepton EDMs are researched. Among them, $\theta_{BB'}$, θ_S , θ_{BL} are all newly introduced ones. The experimental upper limit of electron EDM is $|d_e^{exp}| < 1.1 \times 10^{-29}$ e.cm, which gives strict restrictions on the $U(1)_X$ SSM parameter space. In the our used parameter space, the numerical result of $|d_e|$ can be controlled below the experimental limit. In our study, the largest numerical results of μ EDM and τ EDM are about 2.8×10^{-24} e.cm and 5.0×10^{-23} e.cm respectively. They are all in a reasonable parameter space and do not exceed the upper limit of the experiment. For the corrections of lepton EDMs, the one-loop contributions are dominant. As for the contributions of one-loop and two-loop to EDMs, their relative size ($d_l^{two-loop}/d_l^{one-loop}$) are about $5\% \sim 15\%$ after numerical calculation.

Our numerical results mainly obey the rule $d_e/d_\mu/d_\tau \sim m_e/m_\mu/m_\tau$. In FIG. 3, when $\theta_{BL} = \frac{\pi}{4}$, M_L has a more obvious impact on electron EDM, and the influence of θ_{BL} on electron EDM is also more obvious. In addition, the influences of the CP-violating phases θ_S and $\theta_{BB'}$ on lepton EDMs are also obvious. In FIG. 7, when $\theta_S = \frac{\pi}{3}$, the value of the muon EDM increases as M_E increases (the numerical results are all negative), The θ_S has great influence on the numerical results, because of that M_S is related to the mass matrices of neutralino and charge Higgs. In FIG. 8, when $\theta_{BB'} = \frac{\pi}{6}$, the two lines (solid line, dashed line) are about the decreasing function of M_{E22} . The above parameters (M_L, M_E) are all elements on the diagonal of the mass matrix, so their corresponding results are all decoupled, such as FIG. 3, FIG. 4, FIG. 7, FIG. 8, FIG. 10, FIG. 11. In FIG. 12, We can get that $|d_\tau|$ increases with the increase of $\tan\beta$. If we use the method of mass insertion [46] to analyze the results, it is intuitive to find that $\tan\beta$ is proportional to lepton EDMs. We have also performed some random spot operations on lepton EDMs. The randomly scattered pictures have obvious stratification, also help us to find a reasonable parameter space. As the accuracy of technology improves, lepton EDMs may be detected in the near future.

VI. ACKNOWLEDGMENTS

This work is supported by National Natural Science Foundation of China(NNSFC)(Nos. 11535002, 11705045), Natural Science Foundation of Hebei Province (A2020201002) and the youth top-notch talent support program of the Hebei Province.

Appendix

The mass matrix for slepton with the basis $(\tilde{e}_L, \tilde{e}_R)$

$$m_{\tilde{e}}^2 = \begin{pmatrix} m_{\tilde{e}_L \tilde{e}_L^*} & \frac{1}{2}(\sqrt{2}v_d T_e^\dagger - v_u(\lambda_H v_S + \sqrt{2}\mu) Y_e^\dagger) \\ \frac{1}{2}(\sqrt{2}v_d T_e - v_u Y_e(\sqrt{2}\mu^* + v_S \lambda_H^*)) & m_{\tilde{e}_R \tilde{e}_R^*} \end{pmatrix}, \quad (33)$$

$$\begin{aligned} m_{\tilde{e}_L \tilde{e}_L^*} &= m_{\tilde{l}}^2 + \frac{1}{8} \left((g_1^2 + g_{YX}^2 + g_{YX}g_X - g_2^2)(v_d^2 - v_u^2) + 2g_{YX}g_X(v_\eta^2 - v_{\bar{\eta}}^2) \right) + \frac{1}{2}v_d^2 Y_e^\dagger Y_e, \\ m_{\tilde{e}_R \tilde{e}_R^*} &= m_e^2 - \frac{1}{8} \left([2(g_1^2 + g_{YX}) + 3g_{YX}g_X + g_X^2](v_d^2 - v_u^2) + (4g_{YX}g_X + 2g_X^2)(v_\eta^2 - v_{\bar{\eta}}^2) \right) \\ &\quad + \frac{1}{2}v_d^2 Y_e Y_e^\dagger. \end{aligned} \quad (34)$$

This matrix is diagonalized by Z^E

$$Z^E m_{\tilde{e}}^2 Z^{E,\dagger} = m_{2,\tilde{e}}^{dia}. \quad (35)$$

The mass matrix for CP-even sneutrino (ϕ_l, ϕ_r) reads

$$m_{\tilde{\nu}^R}^2 = \begin{pmatrix} m_{\phi_l \phi_l} & m_{\phi_r \phi_l}^T \\ m_{\phi_l \phi_r} & m_{\phi_r \phi_r} \end{pmatrix}, \quad (36)$$

$$\begin{aligned} m_{\phi_l \phi_l} &= \frac{1}{8} \left((g_1^2 + g_{YX}^2 + g_2^2 + g_{YX}g_X)(v_d^2 - v_u^2) + g_{YX}g_X(2v_\eta^2 - 2v_{\bar{\eta}}^2) \right) \\ &\quad + \frac{1}{2}v_u^2 Y_\nu^T Y_\nu + m_L^2, \end{aligned} \quad (37)$$

$$m_{\phi_l \phi_r} = \frac{1}{\sqrt{2}}v_u T_\nu + v_u v_{\bar{\eta}} Y_X Y_\nu - \frac{1}{2}v_d(\lambda_H v_S + \sqrt{2}\mu) Y_\nu, \quad (38)$$

$$\begin{aligned} m_{\phi_r \phi_r} &= \frac{1}{8} \left((g_{YX}g_X + g_X^2)(v_d^2 - v_u^2) + 2g_X^2(v_\eta^2 - v_{\bar{\eta}}^2) \right) + v_\eta v_S Y_X \lambda_C \\ &\quad + m_{\tilde{\nu}}^2 + \frac{1}{2}v_u^2 |Y_\nu|^2 + v_{\bar{\eta}}(2v_{\bar{\eta}}|Y_X|^2 + \sqrt{2}T_X). \end{aligned} \quad (39)$$

This matrix is diagonalized by Z^R

$$Z^R m_{\tilde{\nu}^R}^2 Z^{R,\dagger} = m_{2,\tilde{\nu}^R}^{dia}. \quad (40)$$

The mass matrix for CP-odd sneutrino (σ_l, σ_r) is also deduced here

$$m_{\tilde{\nu}^I}^2 = \begin{pmatrix} m_{\sigma_l \sigma_l} & m_{\sigma_r \sigma_l}^T \\ m_{\sigma_l \sigma_r} & m_{\sigma_r \sigma_r} \end{pmatrix}, \quad (41)$$

$$\begin{aligned} m_{\sigma_l \sigma_l} = & \frac{1}{8} \left((g_1^2 + g_{YX}^2 + g_2^2 + g_{YX} g_X)(v_d^2 - v_u^2) + 2g_{YX} g_X (v_\eta^2 - v_{\bar{\eta}}^2) \right) \\ & + \frac{1}{2} v_u^2 Y_\nu^T Y_\nu + m_{\tilde{L}}^2, \end{aligned} \quad (42)$$

$$m_{\sigma_l \sigma_r} = \frac{1}{\sqrt{2}} v_u T_\nu - v_u v_{\bar{\eta}} Y_X Y_\nu - \frac{1}{2} v_d (\lambda_H v_S + \sqrt{2} \mu) Y_\nu, \quad (43)$$

$$\begin{aligned} m_{\sigma_r \sigma_r} = & \frac{1}{8} \left((g_{YX} g_X + g_X^2)(v_d^2 - v_u^2) + 2g_X^2 (v_\eta^2 - v_{\bar{\eta}}^2) \right) - v_\eta v_S Y_X \lambda_C \\ & + m_{\tilde{\nu}}^2 + \frac{1}{2} v_u^2 |Y_\nu|^2 + v_{\bar{\eta}} (2v_{\bar{\eta}} Y_X Y_X - \sqrt{2} T_X). \end{aligned} \quad (44)$$

This matrix is diagonalized by Z^I

$$Z^I m_{\tilde{\nu}^I}^2 Z^{I,\dagger} = m_{2,\tilde{\nu}^I}^{dia}. \quad (45)$$

Mass matrix for charginos in the basis: $(\tilde{W}^-, \tilde{H}_d^-), (\tilde{W}^+, \tilde{H}_u^+)$

$$m_{\tilde{\chi}^-} = \begin{pmatrix} M_2 & \frac{1}{\sqrt{2}} g_2 v_u \\ \frac{1}{\sqrt{2}} g_2 v_d & \frac{1}{\sqrt{2}} \lambda_H v_S + \mu \end{pmatrix}, \quad (46)$$

The matrix is diagonalized by U and V

$$U^* m_{\tilde{\chi}^-} V^\dagger = m_{\tilde{\chi}^-}^{dia}. \quad (47)$$

The mass matrix for charged Higgs in the basis: $(H_d^-, H_u^{+,*}), (H_d^{-,*}, H_u^+)$

$$m_{H^-}^2 = \begin{pmatrix} m_{H_d^- H_d^{-,*}} & m_{H_u^{+,*} H_d^{-,*}}^* \\ m_{H_d^- H_u^+} & m_{H_u^{+,*} H_u^+} \end{pmatrix}, \quad (48)$$

$$\begin{aligned} m_{H_d^- H_d^{-,*}} = & \frac{1}{8} ((g_2^2 + g_X^2) v_d^2 + (-g_X^2 + g_2^2) v_u^2 + (g_1^2 + g_{YX}^2) (-v_u^2 + v_d^2) - 2g_X^2 v_{\bar{\eta}}^2 \\ & + 2(g_{YX} g_X (-v_{\bar{\eta}}^2 - v_u^2 + v_d^2 + v_\eta^2) + g_X^2 v_\eta^2) \\ & + \frac{1}{2} (2 |\mu|^2 + 2\sqrt{2} v_S \Re(\mu \lambda_H^*) + v_S^2 |\lambda_H|^2), \end{aligned} \quad (49)$$

$$m_{H_d^- H_u^+} = \frac{1}{2}(2(\lambda_H l_W^* + B_\mu) + \lambda_H(2\sqrt{2}v_S M_S^* - v_d v_u \lambda_H^* + v_\eta v_{\bar{\eta}} \lambda_C^* + \sqrt{2}v_S T_{\lambda_H})) \\ + \frac{1}{4}g_2^2 v_d v_u , \quad (50)$$

$$m_{H_u^{+,*} H_u^+} = \frac{1}{8}((-g_X^2 + g_2^2)v_d^2 + (g_2^2 + g_X^2)v_u^2 + (g_1^2 + g_{YX}^2)(-v_d^2 + v_u^2) - 2g_X^2 v_\eta^2) \\ + 2(g_{YX} g_X (-v_d^2 - v_\eta^2 + v_u^2 + v_{\bar{\eta}}^2) + g_X^2 v_{\bar{\eta}}^2)) \\ + \frac{1}{2}(2|\mu|^2 + 2\sqrt{2}v_S \Re(\mu \lambda_H^*) + v_S^2 |\lambda_H|^2) . \quad (51)$$

This matrix is diagonalized by Z^+

$$Z^+ m_{H-}^2 Z^{+,\dagger} = m_{2,H-}^{dia} . \quad (52)$$

The mass matrix for neutralino in the basis $(\lambda_{\tilde{B}}, \tilde{W}^0, \tilde{H}_d^0, \tilde{H}_u^0, \lambda_{\tilde{X}}, \tilde{\eta}, \tilde{\bar{\eta}}, \tilde{s})$ is

$$m_{\tilde{\chi}^0} = \begin{pmatrix} M_1 & 0 & -\frac{g_1}{2}v_d & \frac{g_1}{2}v_u & M_{BB'} & 0 & 0 & 0 \\ 0 & M_2 & \frac{g_2}{2}v_d & -\frac{g_2}{2}v_u & 0 & 0 & 0 & 0 \\ -\frac{g_1}{2}v_d & \frac{g_2}{2}v_d & 0 & m_{\tilde{H}_u^0 \tilde{H}_d^0} & m_{\lambda_{\tilde{X}} \tilde{H}_d^0} & 0 & 0 & -\frac{\lambda_H v_u}{\sqrt{2}} \\ \frac{g_1}{2}v_u & -\frac{g_2}{2}v_u & m_{\tilde{H}_d^0 \tilde{H}_u^0} & 0 & m_{\lambda_{\tilde{X}} \tilde{H}_u^0} & 0 & 0 & -\frac{\lambda_H v_d}{\sqrt{2}} \\ M_{BB'} & 0 & m_{\tilde{H}_d^0 \lambda_{\tilde{X}}} & m_{\tilde{H}_u^0 \lambda_{\tilde{X}}} & M_{BL} & -g_X v_\eta & g_X v_{\bar{\eta}} & 0 \\ 0 & 0 & 0 & 0 & -g_X v_\eta & 0 & \frac{1}{\sqrt{2}}\lambda_C v_S & \frac{1}{\sqrt{2}}\lambda_C v_{\bar{\eta}} \\ 0 & 0 & 0 & 0 & g_X v_{\bar{\eta}} & \frac{1}{\sqrt{2}}\lambda_C v_S & 0 & \frac{1}{\sqrt{2}}\lambda_C v_\eta \\ 0 & 0 & -\frac{1}{\sqrt{2}}\lambda_H v_u & -\frac{1}{\sqrt{2}}\lambda_H v_d & 0 & \frac{1}{\sqrt{2}}\lambda_C v_{\bar{\eta}} & \frac{1}{\sqrt{2}}\lambda_C v_\eta & m_{\tilde{s}\tilde{s}} \end{pmatrix} , \quad (53)$$

$$m_{\tilde{H}_d^0 \tilde{H}_u^0} = -\frac{1}{\sqrt{2}}\lambda_H v_S - \mu, \quad m_{\tilde{H}_d^0 \lambda_{\tilde{X}}} = -\frac{1}{2}(g_{YX} + g_X)v_d, \\ m_{\tilde{H}_u^0 \lambda_{\tilde{X}}} = \frac{1}{2}(g_{YX} + g_X)v_u, \quad m_{\tilde{s}\tilde{s}} = 2M_S + \sqrt{2}\kappa v_S . \quad (54)$$

This matrix is diagonalized by N ,

$$N^* m_{\tilde{\chi}^0} N^\dagger = m_{\tilde{\chi}^0}^{dia} . \quad (55)$$

[1] N.F. Ramsey, *Rept. Prog. Phys.* **45** 95-113 (1982)

- [2] A. Shindler, *Eur. Phys. J. A* **57** 128 (2021)
- [3] J. Baron, et al., (ACME Collaboration) *Science* **343** 269 (2014)
- [4] V. Andreev, et al., (ACME Collaboration) *Nature* **562** 355-60 (2018)
- [5] A. Crivellin, M. Hoferichter, P.S. Wellenburg *Phys. Rev. D* **98** 113002 (2018)
- [6] P.A. Zyla, et al.,(Particle Data Group), *PTEP* **8** 083-01 (2020)
- [7] F. del Aguila, M. B. Gavela, J. A. Grifols, et al., *Phys. Lett. B* **126** 71-73 (1983); Erratum: *Phys. Lett. B* **129** 473 (1983)
- [8] T. Ibrahim, P. Nath, *Phys. Rev. D* **58** 111301 (1998); Erratum: *Phys. Rev. D* **60** 099902 (1999)
- [9] S. Atag, E. Gurkanli, *JHEP* **1606** 118 (2016)
- [10] T. Abe, N. Omoto, O. Seto et al., *Phys. Rev. D* **98** 075029 (2018)
- [11] J. Rosiek, *Phys. Rev. D* **41** 3464 (1990)
- [12] H.P. Nilles, *Phys. Rept.* **110** 1 (1984)
- [13] H.E. Haber, G.L. Kane, *Phys. Rept.* **117** 75 (1985)
- [14] S.M. Zhao, T.F. Feng, X.J. Zhan, et al., *JHEP* **07** 124 (2015)
- [15] F. Staub, SARAH, (2008) arXiv:0806.0538
- [16] F. Staub, *Comput. Phys. Commun.* **185** 1773 (2014)
- [17] F. Staub, *Adv. High Energy Phys.* **2015** 840780 (2015)
- [18] M. Carena, J.R. Espinosaos, C.E.M. Wagner, et al., *Phys. Lett. B* **355** 209 (1995)
- [19] M. Carena, S. Gori, N.R. Shah, et al., *JHEP* **1203** 014 (2012)
- [20] S. Heinemeyer, D. Stockinger and G. Weiglein, *Nucl. Phys. B* **699** 103 (2004)
- [21] T.F. Feng, T. Huang, X.Q. Li, et al., *Phys. Rev. D* **68** 016004 (2003)
- [22] M. Pospelov, A. Ritz, *Annals Phys.* **318** 119-169 (2005)
- [23] T. Abe, J. Hisano, T. Kitahara, K. Tobioka, *JHEP* **1401** 106 (2014)
- [24] S. Ipek, *Phys. Rev. D* **89** 073012 (2014)
- [25] W. Bernreuther, L. Chen, O. Nachtmann, *Phys. Rev. D* **103** 096011 (2021)
- [26] A. Pilaftsis, *Phys. Rev. D* **58** 096010 (1998)
- [27] M. Carena, J. Ellis, A. Pilaftsis, et al., *Nucl. Phys. B* **586** 92 (2000)
- [28] N. Yamanaka, *Phys. Rev. D* **87** 011701 (2013)

- [29] X.G. He, C.J. Lee, S.F. Li, J. Tandean, *JHEP* **1408** 019 (2014)
- [30] X.G. He, C.J. Lee, S.F. Li, J. Tandean, *Phys. Rev. D* **89** 091901 (2014)
- [31] S.M. Zhao, T.F. Feng, M.J. Zhang, et al., *JHEP* **02** 130 (2020)
- [32] M.E. Peskin, D.V. Schroeder, An introduction to quantum field theory, Addison Wesley: Reading U.S.A. (1995)
- [33] G. Belanger, J.D. Silva, H.M. Tran, *Phys. Rev. D* **95** 115017 (2017)
- [34] V. Barger, P.F. Perez, S. Spinner, *Phys. Rev. Lett.* **102** 181802 (2009)
- [35] P.H. Chankowski, S. Pokorski, J. Wagner, *Eur. Phys. J. C* **47** 187 (2006)
- [36] L.H. Su, S.M. Zhao, X.X. Dong, et al., *Eur. Phys. J. C* **81** 433 (2021)
- [37] T.F. Feng, L. Sun, X.Y. Yang, *Nucl. Phys. B* **800** 221-252 (2008)
- [38] X.Y. Yang, T.F. Feng, *Phys. Lett. B* **675** 43 (2009)
- [39] CMS collaboration, *Phys. Lett. B* **716** 30 (2012)
- [40] ATLAS collaboration, *Phys. Lett. B* **716** 1 (2012)
- [41] Particle Data collaboration, Review of Particle Physics, *Prog. Theor. Exp. Phys.* **2020** 083C01 (2020)
- [42] ATLAS collaboration, *Phys. Lett. B* **796** 68 (2019)
- [43] G. Cacciapaglia, C. Csáki, G. Marandella and A. Strumia, *Phys. Rev. D* **74** 033011 (2006)
- [44] M. Carena, A. Daleo, B.A. Dobrescu and T.M.P. Tait, *Phys. Rev. D* **70** 093009 (2004)
- [45] L. Basso, *Adv. High Energy Phys.* **2015** 980687 (2015)
- [46] T. Moroi, *Phys. Rev. D* **53** 11 (1996)